Multilayer Coatings for High-Energy Optics for Astrophysics

Characterization of a W/Si graded multilayer coated mirror shell (n. 333) preformed by Nickel electroforming

*Mirror shell X-ray reflectivity measured at the PANTER facility by **W. Burkert** and **G. Hartner** (MPE)*

*Witness mirror characterization by **D. Vernani** and **R. Canestrari** (INAF/OAB)*

*AFM scans taken by **R. Valtolina** (INAF/OAB)*

*Reflectivity data analysis by **D. Spiga** (INAF/OAB)*

Issued by:	Name:	Dr. D. Spiga INAF-OAB	Signature:		Date:	2005
Reviewed by:	Name:	Dr. G. Pareschi INAF-OAB	Signature:		Date:	2005

Table of Contents

1. Optic test at the PANTER facility

The aim of this document is the exposition of the characterization of the reflectivity of an hard X-ray optic prototype, performed on a hard X-ray mirror shell with a *graded* W/Si multilayer coating. The X-ray shell (named shell **333**) was produced in the context of a collaboration between INAF/OAB and the Harvard-Smithsonian Center for Astrophysics (*CfA* Boston, USA): this research is aimed to the production of a prototype of the optics for Con-X/HXT, following the approach of deposition of the multilayer reflective coating in an already replicated substrate. The mirror substrate was produced by Nickel electroforming and afterwards coated with a W/Si broadband multilayer, constituted by two power laws of d-spacings: the deepest one has 75 bilayers with d-spacing ranging from 40 to 28 Å and it is devoted to the reflection of the hardest X-rays, while the outer one has 20 thicker bilayers with d-spacings from 126 to 38 Å and reflects the softest X-rays.

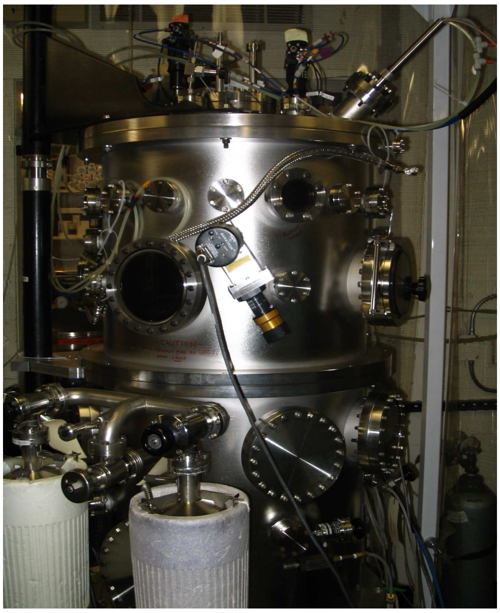

Fig.1: the magnetron sputtering coating facility at the Harvard-Smithsonian Center for Astrophysics (credits: CfA). Outside view ***(left)****, inside view* ***(right)****: a Nickel cylindrical mirror shell is visible between the magnet pole pieces.*

1 Preliminary information

The considered optic has a Wolter I profile, with the following features:

- maximum mirror diameter: (2r): 231 mm
- minimum mirror diameter: 226 mm
- mirror length: 2L = 426.5 mm
- on-axis incidence angle: α = 0.164°
- mirror walls thickness: 100 µm

Note, in particular, the extreme small thickness of the mirror walls, a factor of merit for lightweight optics to be installed aboard spacecrafts, but at cost of the optic rigidity and, consequently, of the imaging quality.
The focal length (for an infinite distance source) is, thus, 10 m and the on-axis collecting geometric area is then $8\pi Lf\alpha^2$ = 5.82 cm^2: however, the finite source distance (X_s = 121 m) causes a beam divergence at the mirror of θ = 0.054°, and the image is formed at a distance X_i = 10.9 m from the mirror principal plane,

$$\frac{1}{X_s} + \frac{1}{X_i} = \frac{1}{f}$$

for the same reason, incoming X-rays strike of the hyperbola and on the parabola with two different grazing angles:

- actual incidence angle on the parabola: $\alpha+\theta = 0.218°$
- actual incidence angle on the hyperbola: $\alpha-\theta = 0.110°$

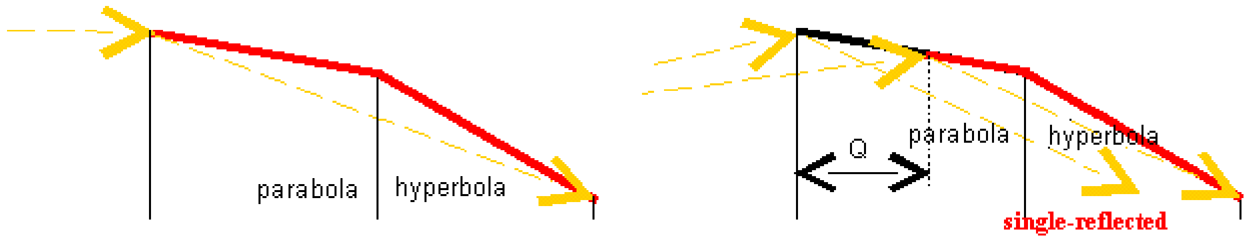

Fig. 2: An effect of the finite source distance: the X-rays reflected by the front-end of the paraboloid are not reflected by the hyperbola and they are focused at a distance 2f. For double reflection a area fraction Q is lost.

consequently, the reflectivities of the two surfaces will be also different: $R_H^{\alpha-\theta}(E) \neq R_P^{\alpha+\theta}(E)$, and the mirror cross-section for double reflection will be also different:

$$A_g = 2\pi Lr\,(\alpha+\theta)\ (1-Q)\ (1-V)$$

where V = 10% accounts for the spider vignetting and the factor Q takes into account the single-reflected rays by the parabola that miss the reflection on the hyperbola (fig. 2). The factor Q has the expression:

$$Q = \frac{8f}{X_s + 4f}$$

and in this case, is equal to 49%. It can be, moreover, easily verified (simply substitute in the 1-Q definition f = r/4α and Xs = r/θ) that A_g is exactly the area of the hyperboloid cross-section seen by the parabola-reflected wavefront:

$$A_g = 2\pi Lr\,(\alpha-\theta)\ \ (1-V)$$

The mirror effective area can be, thus, evaluated as

$$A_{eff} = R_H^{\alpha-\theta}\, R_P^{\alpha+\theta} 2.67\ \mathrm{cm}^2$$

the product of the two reflectivities $R_H^{\alpha-\theta}\, R_P^{\alpha+\theta}$ at different energies can so be calculated from the mirror effective area as a function of the photon energies,

$$A_{eff}(E) = \frac{C_c(E)}{B_{inc}(E)}$$

$$R_p(E)R_h(E) = \frac{A_{eff}(E)}{A_g}$$

which is known from the ratio of the collected (focused) photons C_c(E) and the incident photon flux density B_{inc}(E):

$$A_{eff}(E) = \frac{C_c(E)}{B_{inc}(E)}$$

B_{inc}(E) is known from a flat field measurement, prior to the mirror illumination.

2 Witness mirror reflectivity measurement

A preliminary evaluation of the coating reflectivity has been performed on a witness mirror sample by S. Romaine at 8.05 keV: the considered sample is a fused silica substrate with excellent initial smoothness (< 1 Å), so we can expect a much better multilayer roughness for the witness than for the shell: also the multilayer structure will be slightly different since mirror shell and witness sample were placed at different locations in the coating chamber. The reflectivity can be well modeled (see fig. 3) with a roughness rms σ = 3-4 Å.

Fig. 3: the witness mirror reflectivity scan at 8.05 keV (log plot) . The reflectance scan can be fitted assuming an average roughness rms of 3-4 Å.

Assuming the inferred mirror structure, we can simulate the expected two-reflection reflectivity of the mirror shell within the detector acceptance angle, for different rms roughness values (that in the mirror shell case will be surely much larger) in the spatial frequency sensitivity window (fig. 4).

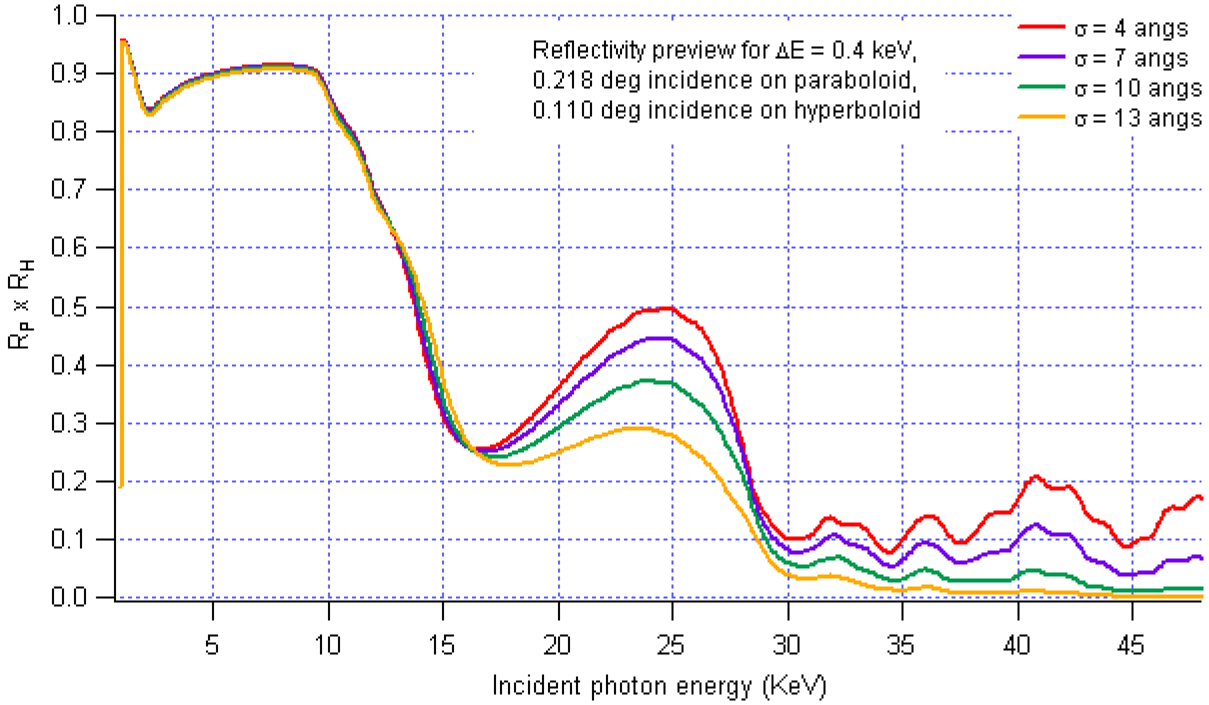

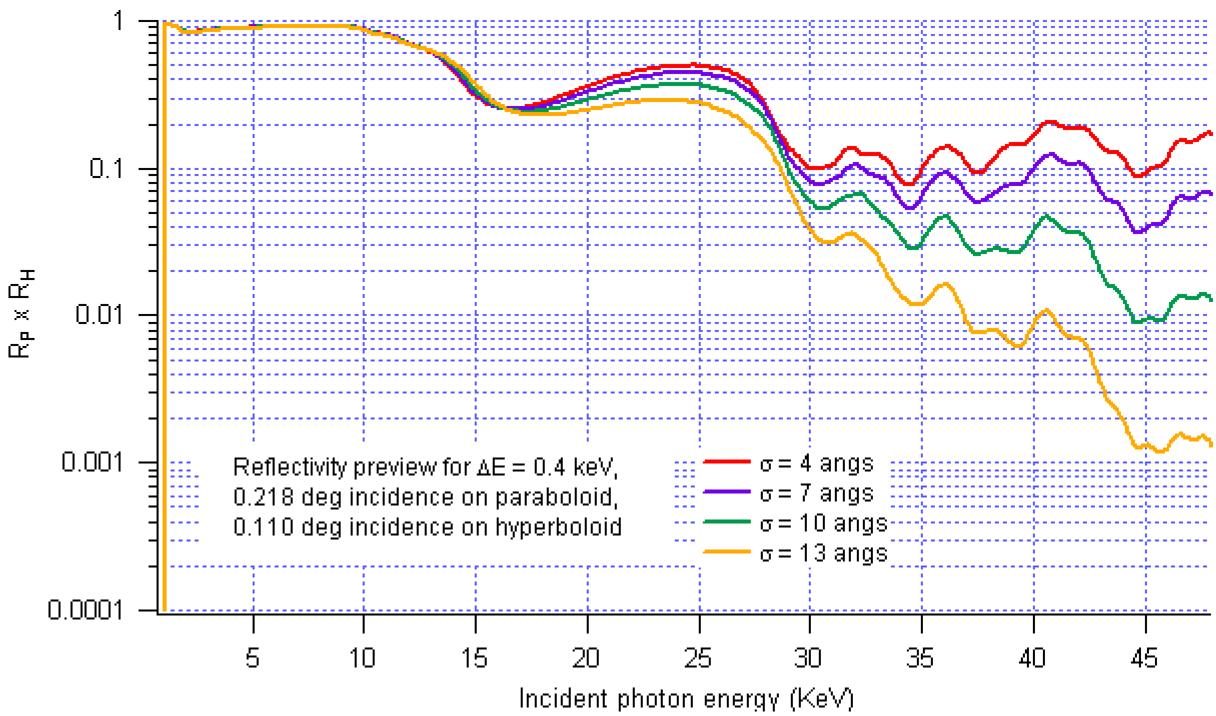

Fig. 4: simulated reflectivity of the mirror shell (double reflection hyperbola +parabola) for different values of the multilayer roughness rms. The listed rms values are to be fitted considering the acceptance angle of the detector. Linear plot (top) and logarithmic plot (below).

3 Panter reflectivity measurements

a) low energy measurements (PSPC detector)

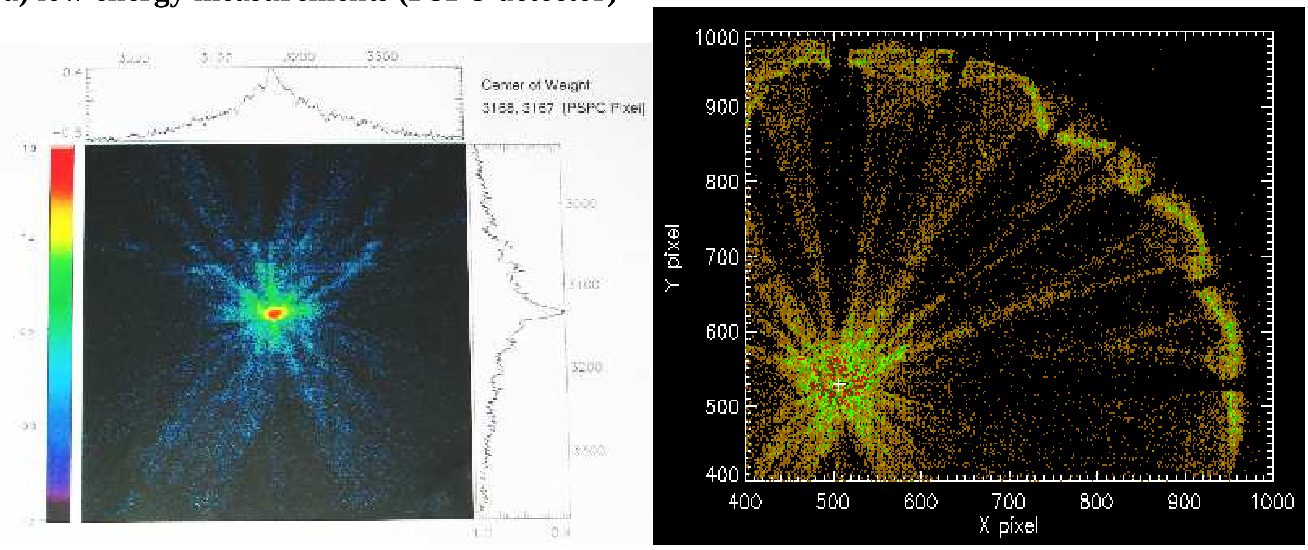

Fig. 5: the focal spot observed with the PSPC detector at the Ti-K line energy (4.51 keV):
(left) *close view on the focal spot: it appears to be elongated in the horizontal direction and a large amount of scattering is visible: moreover, the radial structure of scattered photons seems to suggest an important deformation of the mirror shell in correspondence to the spider arms bonding (PANTER image, logarithmic color scale).*
(right) *a larger PSPC field: also the corona caused by the single reflection is visible, showing clearly the deformations of the mirror profile. The black circle is due to the PSPC wires texture. Note the formation of radial scattering in correspondence to the mirror segments (logarithmic color scale).*

The reflectivity measurement was performed first at low energies (< 10 keV) using the PSPC detector. Despite its very poor energy resolution (20%), this counting device is particularly suitable to perform HEW measurements in monochromatic setup since it does not saturate: moreover, the low, monochromatic energies at which the measurement is done allow the minimization of the scattering caused by the surface microroughness (scaling roughly as $\sigma^2 \lambda^{-2}$): the HEW we measure with the PSPC is thus essentially due to the profile deformations, i.e., to the low-frequencies deviation from the ideal profile.

The measurements, performed at several energies (see tab.1), highlighted the presence of important deformation of the mirror, especially in correspondence to the spider arms where the shell is bonded. This is visible (see fig. 5) from the single- reflection corona formed around the focal spot. Also an important part of scattering is visible in the PSPC field as radial structures, meaning that the X-ray scattering is mainly located in the incidence plane, which is typical of scattering from surface microroughness. After achieving the best focus distance (that turned out to be 10.90 m, as expected), the Half Energy Width of the focal spot has also been measured at the listed energies in the tab.1. The HEW is larger for increasing energies, as expected. However, it should be noted that the choice of the Region Of Interest (ROI) affects strongly these values since the X-ray scattering is extended over all (and also outside) the PSPC field.

The choice of the ROI affects, indeed, also the reflectivity measurement: a small integration box would cause an important fraction of scattered rays at large angles to be excluded from the integration, and would underestimate the integral reflectivity of the mirror. The choice of a too large ROI is also, however, a non-viable solution because it causes the inclusion of a number of single-scattered X-rays from the single-reflection on the parabola, and would lead to the overestimate of the effective area for double reflection. The reflectivity values measured with the PSPC detector are shown in fig. 7: the red triangles are the reflectivity measurements in a circular ROI with a 250 pixels radius, corresponding to 21.7 mm (i.e. 450" from the mirror principal plane): they underestimate the assumed model, while the blue triangles are calculated for a larger ROI (400 pixels, radius, i.e. 34.7 mm, i.e. 650" seen from the mirror) and overestimate the theoretical model because it includes also a non negligible fraction of single-reflected rays.

X-ray line	Energy (keV)	HEW (arcsec)
C-K	0.27	78.9
Cu-L	0.93	73.5
Al-K	1.49	80.5
Ti-K	4.51	83.3
Cu-K	8.05	83.4
Cr-K	5.41	111.5
Fe-K	6.40	111.0

Tab. 1: the mirror shell HEW observed with the PSPC detector. The values are measured within a 200 x 200 pixel box, except the last two (430 x 430).

b) high energies measurements (pn-CCD camera)

The reflectivity measurements were also performed in energy-dispersive setup, using the bremsstrahlung continuum emitted by a W anode powered at 10, 20, 30, 50 kV, in order to cover an energy range from 5 to 50 keV of incident X-ray photons. The collected photons have been observed using the pn-CCD camera in energy-dispersive setup: from the formulas on page 5 it is thus possible to derive the (product of) reflectivities channel by channel, over a wide energy range. The focal spot in fig. 6 is obtained with an exposure of the mirror to X-rays up to 30 keV: when compared to the figure 5, a much larger amount of scattering is visible in the pn field.

The product of the reflectivities is plotted in fig. 7. The superposition of data in the overlapping spectral regions is apparent. To calculate the reflectivity, we have assumed as integration ROI a square of 40 mm around the focal spot: this value corresponds to the maximum size for the integration region without including the single-reflected photons. The integration area is thus 1600 mm^2 – more exactly, 1500 mm^2 if we subtract the pn-CCD dead area, - and it turns out to be quite near to the PSPC area considered in the small box case (1385 mm^2). We can so expect that the pn reflectivity values will be in agreement to the PSPC data calculated in the small box case: this agreement is apparent in fig. 7 (overlapping red triangles – green crosses).

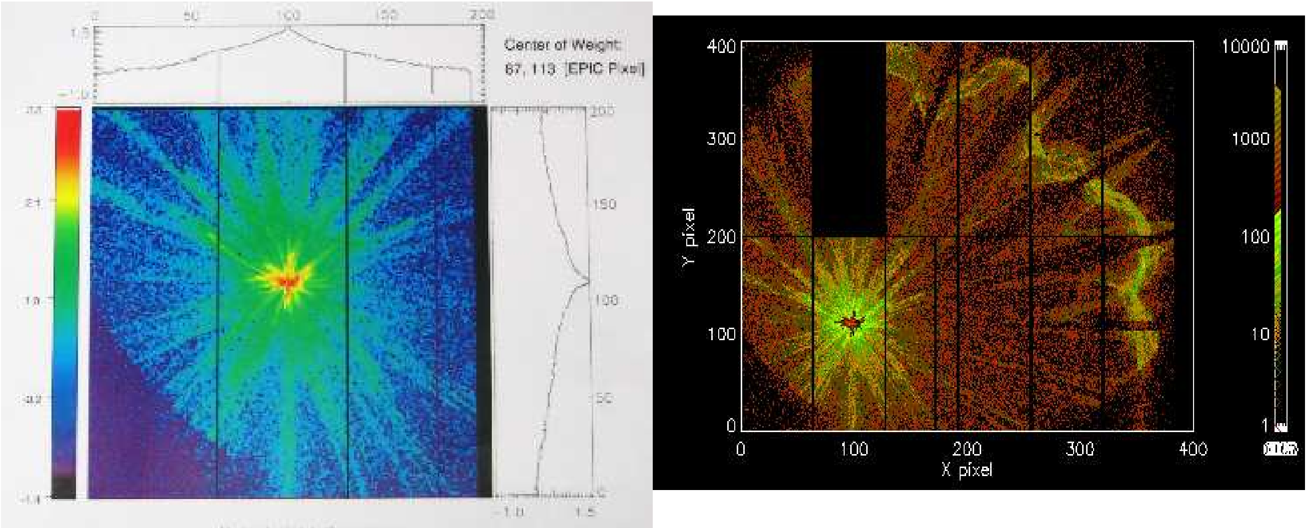

Fig. 6: the focal spot observed with the PN camera, at photon energies from 10 to 30 keV. ***(left)*** *close view on the focal spot: a larger scattering amount is visible in all directions (PANTER image).* ***(right)*** *the full PSPC field (6 cm x 6 cm) showing also the outer, single-reflection corona. All images have a logarithmic color scale.*

The average reflectivity profile as a function of energy can be represented by a model that assumes the same structure of the multilayer in the witness mirror, but with a roughness rms between 20 and 25 Å (see fig. 7). The details of the multilayer structure (with eventual differences between witness and shell) cannot be determined by the fit because the large roughness suppresses many reflectance structures. The agreement is good between 20 and 30 keV, while at lower energies the model overestimates the pn data. At energies beyond 30 keV (and up to 40 keV at least), instead, the model underestimates the pn data.
This disagreement can be a combined effect of the large integration box and of the intense X-ray scattering: for a definite surface/interface spatial wavelength *l* (corresponding to a definite value of the surface/interface PSD) harder photons are more strongly scattered, but mainly inside the Region of Interest: keeping constant the surface/interface PSD, softer photons are affected by a less intense overall scattering, but at larger angles, in agreement with the classical grating formula:

$$l = \frac{1}{f} = \frac{\lambda}{|\cos\theta_s - \cos\theta_i|}$$

At lower energies, we are missing an important part of the photon flux because they are scattered out of the detector sensitive area. Hence, since the agreement measurement/model with 25 Å of rms is good around 20 keV corresponding to a spatial wavelength of for a scattering at the edge of the ROI (2 cm off-axis), we can assume that the multilayer roughness is 25 Å at spatial frequencies beyond $[0.5\ \mu m]^{-1}$.

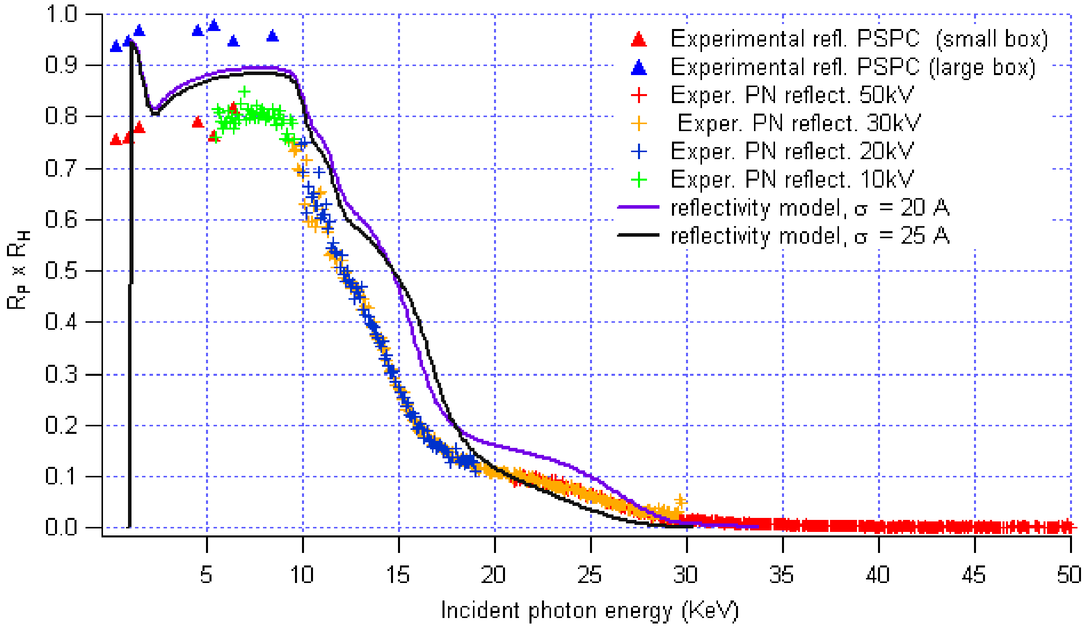

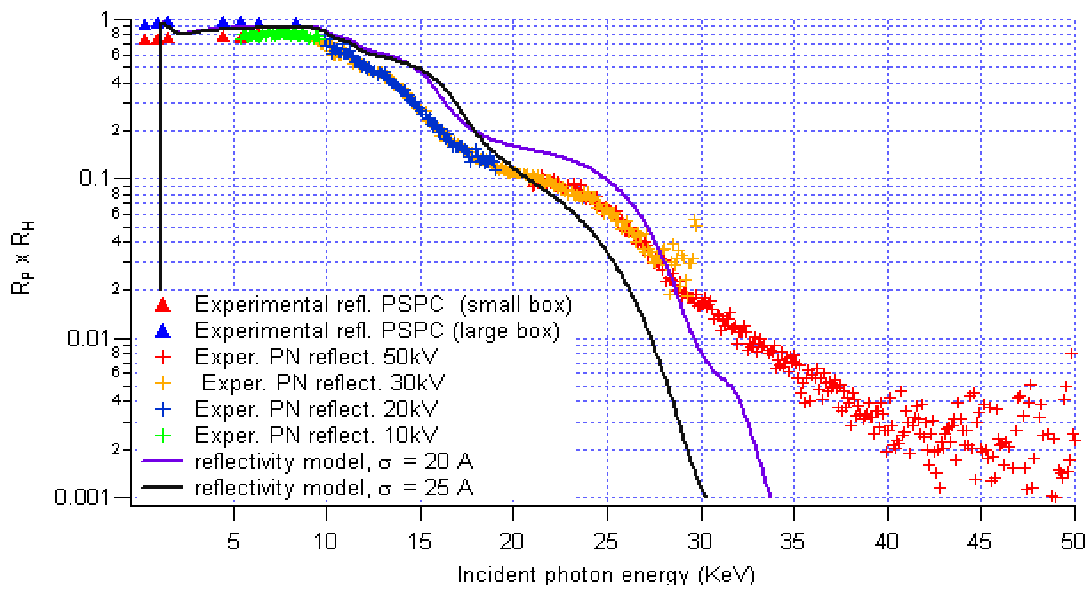

Fig. 7: the measured product of the reflectivities of parabola and hyperbola using a energy-dispersive setup (pn-CCD + bremsstrahlung incident spectrum), represented with "+" markers.
(above) *linear plot.*
(below) *logarithmic plot*
The triangles represent the reflectivity measured with PSPC + monochromatic X-ray lines. The consistency of the experimental data is good provided that they are referred to the same size of the integration box (pn + red triangles). When we adopt a too large box, however (blue triangles), a part of the scattering from the single reflection is also included and the measured value overestimates the theoretical reflectance.

4 Performed measurements at OAB (AFM, WYKO, XRS)

We have also performed at INAF/OAB some metrological tests of some shell samples: for practical reasons it was not possible to analyze the same shell tested at PANTER, but tests have been done using an identical mirror shell replicated from the same mandrel and coated with the same multilayer deposited with the same magnetron sputtering facility.
The X-ray scattering test @ 8.05 keV has given a first evidence of ***anisotrophy*** of the sample: in fig. 8 two X-ray scattering scans are plotted: both were done with the same X-ray beam and in particular with the same incidence angle (0.59º, in correspondence to the first reflectivity maximum after the external reflection region). However, the red plot has been taken with the X-ray beam incident in the optical axis plane, while the black plot is obtained with the X-ray beam incident in the azimuthal plane of the optic. We observe in the second case a much intense scattering (on average, a 4-fold factor) at low angle (in particular up to 0.5º away from the specular beam, corresponding to a spatial wavelength of 0.4 µm). Since the multilayer interfaces PSD is proportional to the intensity of scattering, we can conclude that up to the spatial wavelength of 0.4 µm, the roughness PSD is 4 times larger in the azimuthal direction than in the axial direction. This evidence of anisotrophy indicates, moreover, that a large amount of the multilayer roughness can be caused by the initial roughness of the substrate.

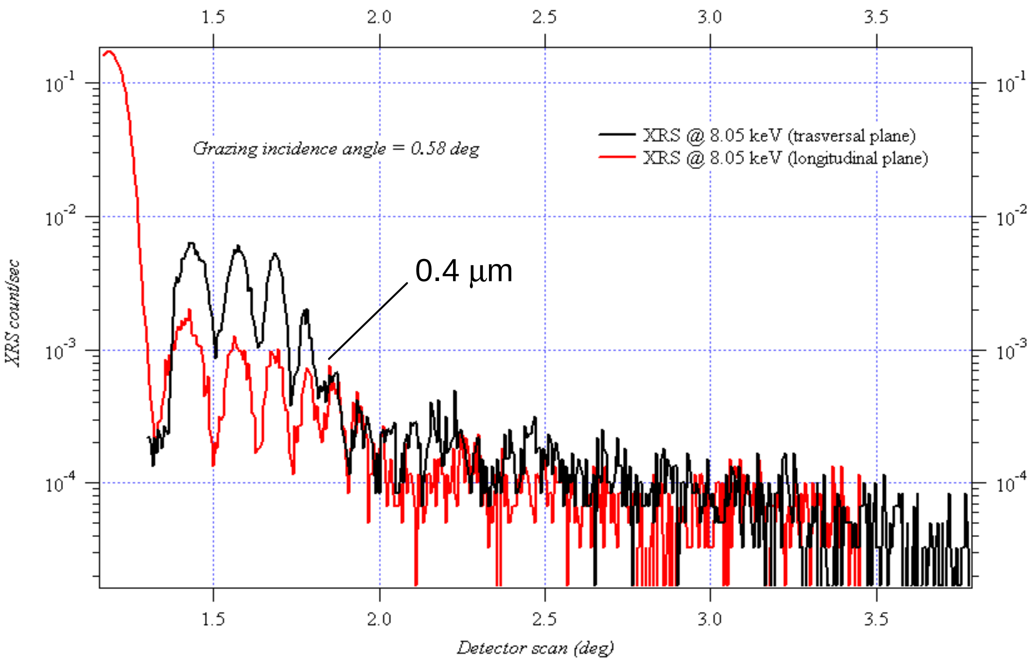

Fig. 8: X-ray scattering at 8.05 keV of a similar mirror shell sample (5 cm x 5 cm) coated with the same multilayer. The two scattering measurements are done at the same grazing incidence angle (0.58 deg), where the reflectivity has a broad maximum. The black plot is obtained orienting the X-ray beam in the azimuthal direction, while the red plot represents the XRS from the same surface, but orienting the X-ray beam in the axial direction. The strong difference indicates that the sample is anisotropic, and in particular the roughness is larger in the azimuthal plane.

Also topographical investigations of the multilayer properties have been done, using the WYKO profilometer installed at INAF/OAB. Several profiles extracted in the axial and azimuthal direction have shown different properties (see fig. 9): the amplitude of defects is much larger for profiles in azimuthal direction, showing a number of features in injection (scratches mainly axially oriented). The resulting rms of the surface in the two directions is 4 Å (axial section) and 11 Å (azimuthal section): the same result can be obtained from the spectral analysis of the measured profiles (fig. 10), that shows, in addition, a major anisotrophy at the lowest frequencies in the WYKO sensitivity window.

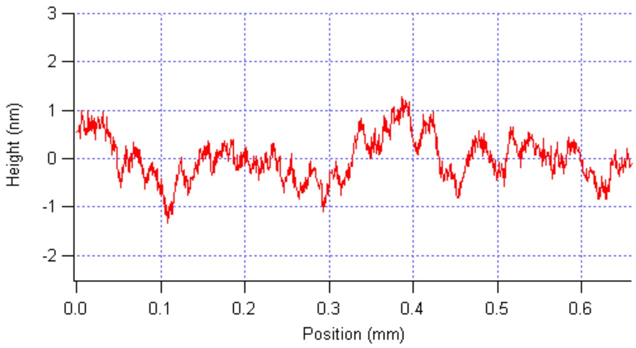

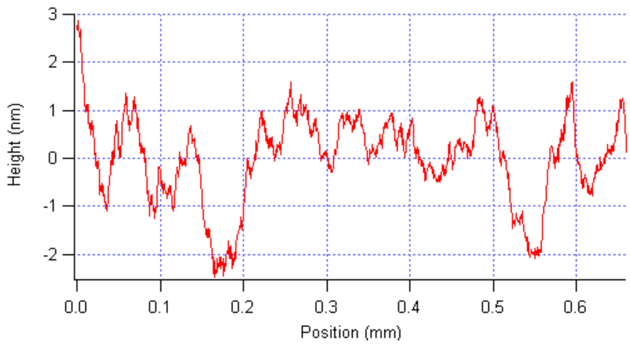

Fig.9: two WYKO profiles of the mirror shell sample under test. ***(left)*** *axial section and* ***(right)*** *azimuthal section. The two graphs have the same vertical axis scale.*
The corresponding rms are respectively 0.4 and 1.1 nm. We can observe, from the profile topography, that the azimuthal profile has a much larger amplitude at low frequencies, since it presents much deeper "grooves", that should be visible in the 2D imaging as "scratches" oriented in the axial direction.

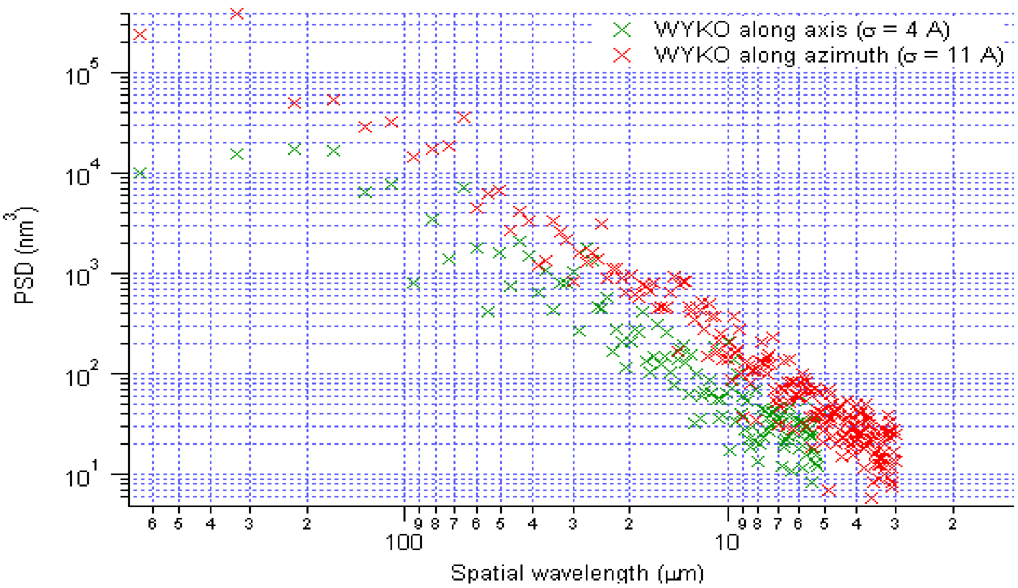

Fig. 10: Power Spectral Density (PSD) of a number od WYKO scans of the mirror-shell sample mentioned above, measured along axial (green) and azimuthal (red) directions. The sample anisotrophy is apparent. The anisotrophy is larger at the lowest frequencies, and the prevalence of axially-oriented defects could be responsible also for the out-of plane scattering which is seen in PANTER images.

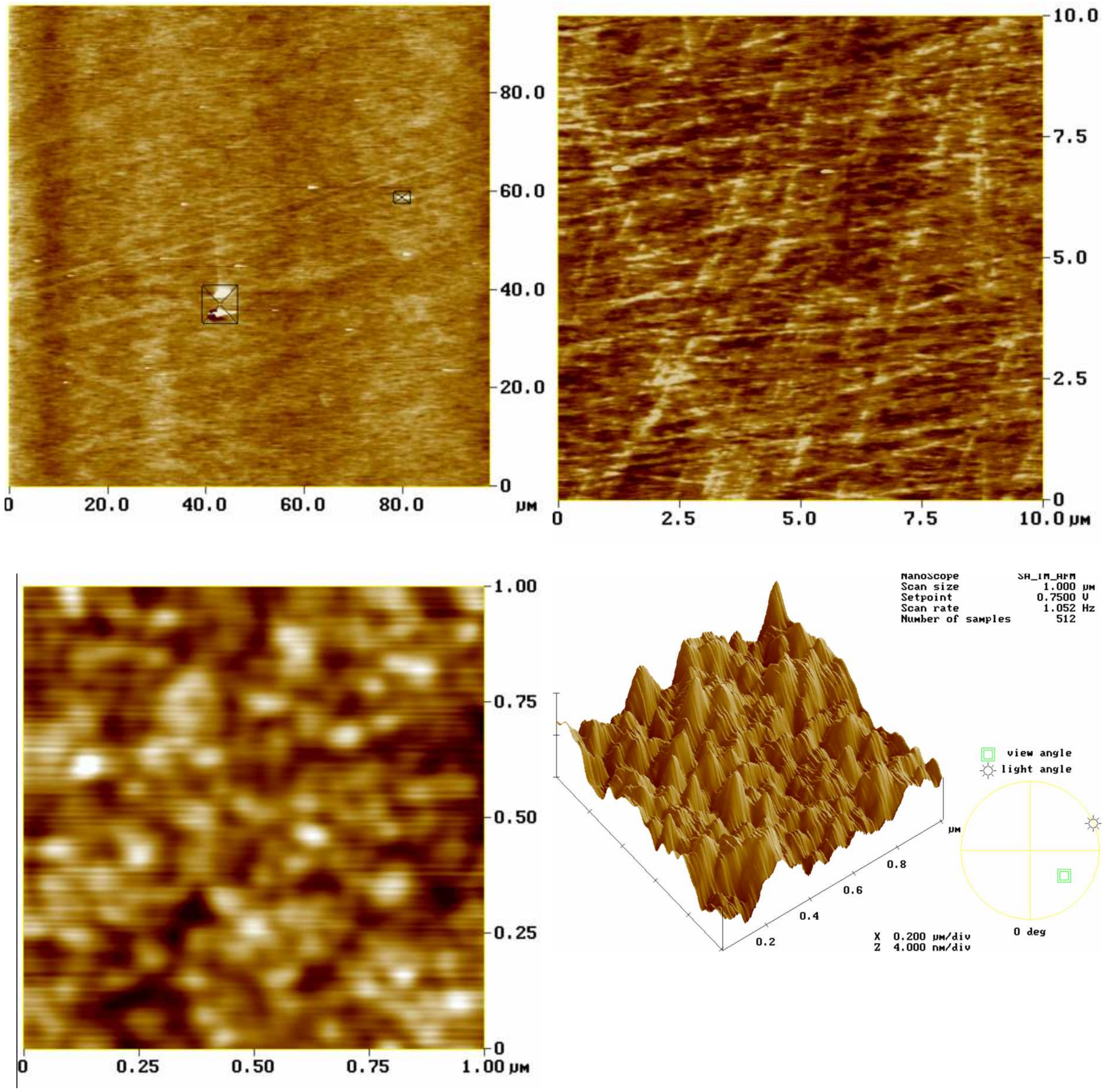

Fig. 11: Some AFM scans taken on a piece of the mirror shell sample.
*(**Above**): 100 µm and 10 µm maps (2D): clear scratches appear on the surface: these features are already present on the mandrel used to replicate the substrate and they are replicated to the Gold layer and, durng the multilayer deposition, to the multilayer coating.stack The obtained rms values are 5 Å and 10 Å, respectively: the larger roughness present in the smaller scan can be a consequence of the multilayer roughness growth.*
*(**below**): 1 µm map (2D and 3D). the surface texture is constituted by nucleations and columnar structures, rather than scratches. The Rms value is 10 Å, a rather large value when compared to the 100 an 10 µm scans. At these spatial frequencies, roughness features are no more anisotropic.*

Also the AFM technique has been used to estimate the multilayer roughness (see fig. 11). The 100 and 10 μm wide scans present clear scratches, with a preferential axial orientation which is more evident in the former. Also with the AFM the anisotrophy seems to be reduced for increasing spatial frequencies, and it disappears in 1 μm wide scans, leaving room to typical nucleations, that could be related to the multilayer growth process. The rms values are 5 Å, 10 Å and 10 Å for 100, 10, 1 μm wide scans respectively.